Measuring Coherent Polarimetric Backscatter Time-Series Covering 1-40 GHz with the ESA WBSCAT Scatterometer

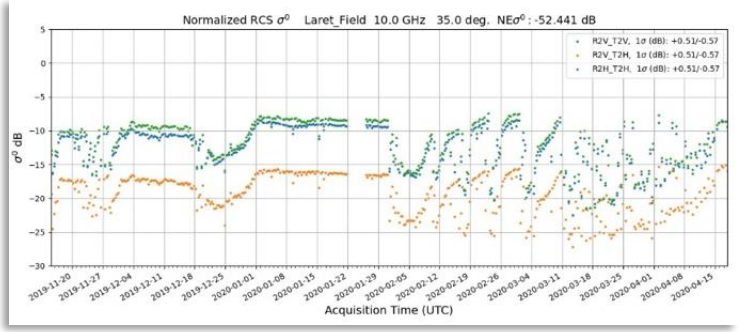

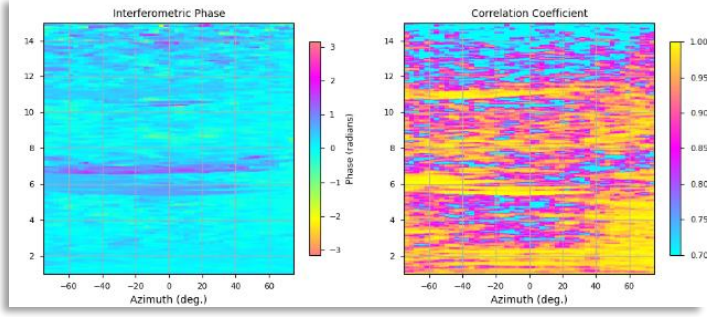

Charles Werner[1], Andreas Wiesmann[1], Rafael Caduff[1], Silvan Leinss[1], Othmar Frey[1], Urs Wegmüller[1], Mike Schwank[1], Christian Mätzler[1], and Martin Suess[2]

[1]Gamma Remote Sensing AG, Worbstrasse 225, Gümligen, Switzerland

[2]ESA ESTEC Noordwijk, Netherlands

10th EARSeL Workshop on Land Ice and Snow, 6-8 Feb., Bern, Switzerland

Introduction

- WBSCAT is a ground-based coherent and fully polarimetric microwave scatterometer operating over the frequency range of 1-40 GHz
- WBSCAT project (ESA/ESTEC Contract 4000121522) began 2017, deployed Dec. 2018 at Davos-Laret
- Snow and agricultural fields exhibit strong variations in the radar signature as a function of time, frequency, and polarization. Detailed microwave measurements combined with concurrent in-situ data of the objective variables is useful for retrieval algorithm development and validation
- Follow-on to the ESA SnowScat Scatterometer operating over the 9-18 GHz. Both lower and higher frequencies are of interest

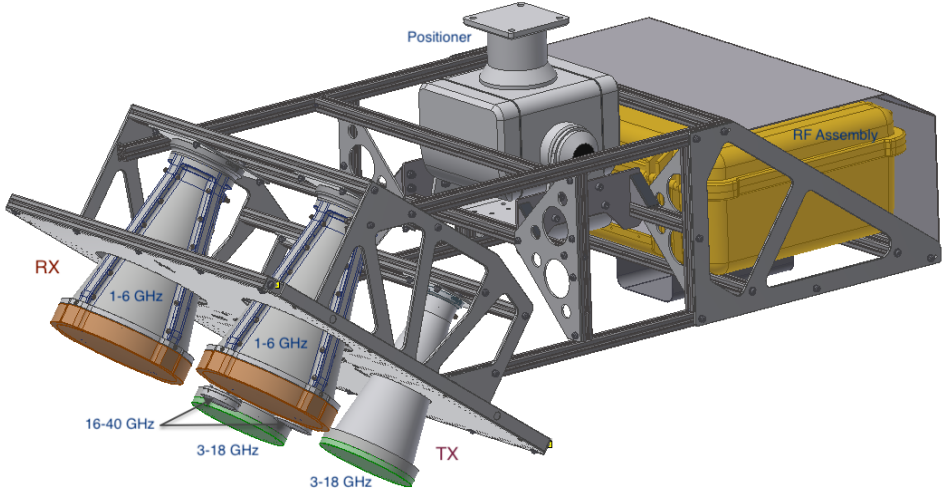

WBSCAT System Design

- Vector Network Analyzer based design. Additional amplifiers for the receiver and transmitter to improve receiver noise figure and SNR
- There are 3 overlapping frequency bands: 1-6, 3-18, and 16-40 GHz, using three quad-ridge dual-pol horn antennas

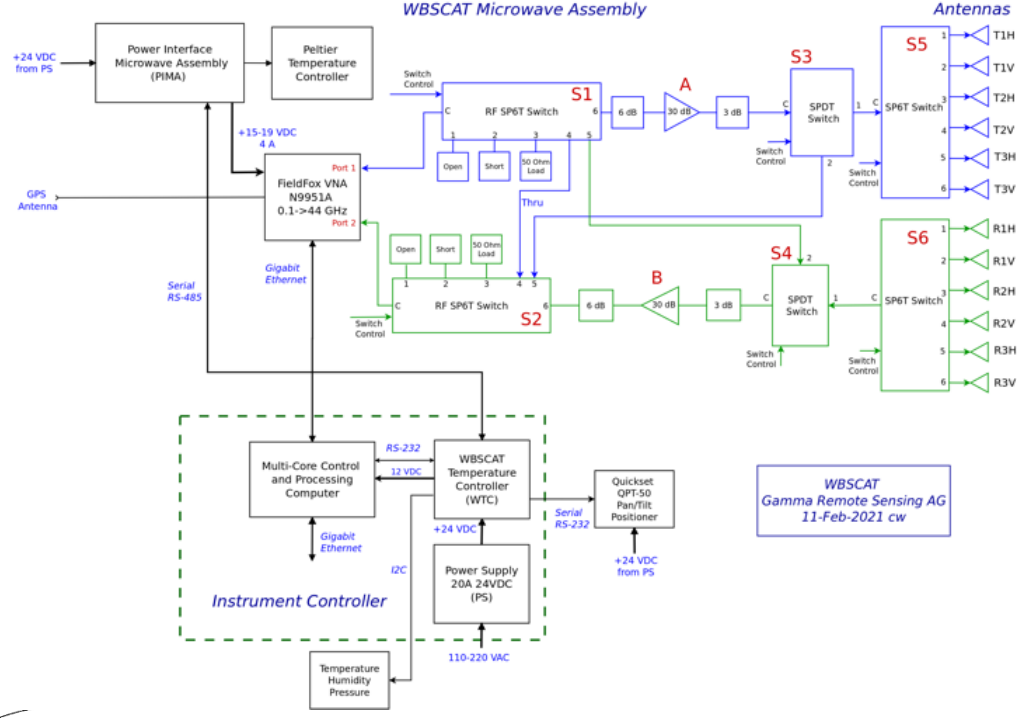

Internal WBSCAT Calibration

- Calibrate the VNA using **S**hort **O**pen **L**oad **T**hru (SOLT) characterization with external standards
- Measure the TX and RX amplifier S-Parameters with the VNA

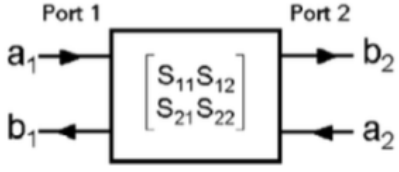

$$\begin{bmatrix} b_1 \\ b_2 \end{bmatrix} = \begin{bmatrix} S_{11} & S12 \\ S_{21} & S_{22} \end{bmatrix} \begin{bmatrix} a_2 \\ a_2 \end{bmatrix}$$

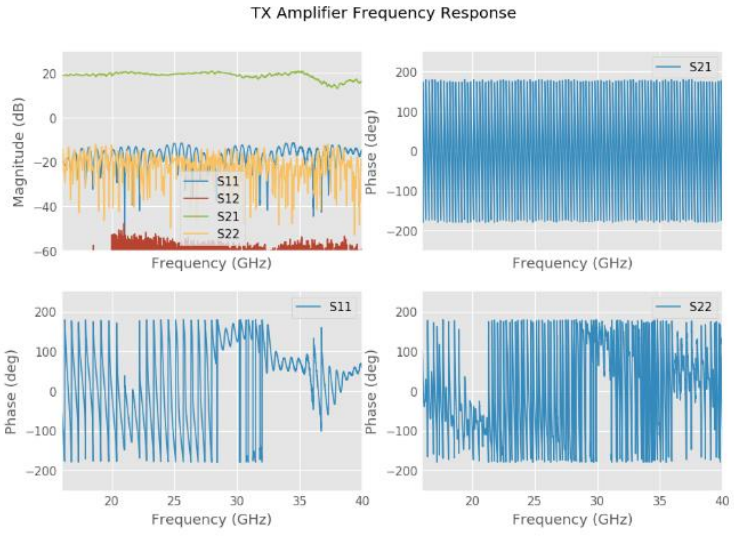

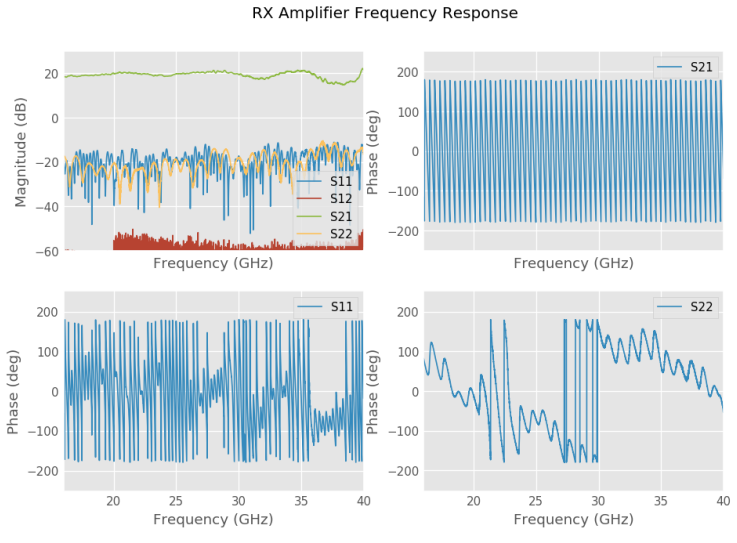

Range-Compression of the Frequency Sweep Backscatter

- The raw data are processed into sub-bands with specified center frequency and bandwidth
- Range compression should oversample the data by a factor of at least 2 by default
- A Kaiser window is applied to the sub-band data to reduce sidelobes:

$$f_{BP}(t) = \frac{e^{j\omega_c t}}{W_0}\frac{\Delta\omega}{2\pi}\sum_{-\frac{N}{2}}^{\frac{N}{2}} F_{BP}(\omega_c + n\Delta\omega)W(n\Delta\omega)e^{j(n\Delta\omega)t}$$

- The time variable $\mathbf{t}$ can be converted to an equivalent monostatic distance r: $r = \frac{ct}{2}$

- The window function W(n) has the same number of samples as the selected spectral window covering the desired bandwidth. The renormalization factor W_0 compensates for signal lost by the window and is given by:

$$W_0 = \frac{\Delta\omega}{2\pi}\sum_{-\frac{N}{2}}^{\frac{N}{2}} W(n\Delta\omega)$$

Range-Compressed Bandpass-Filtered Backscatter

- Range compressed data are corrected for cable and antenna propagation delays, $\beta = 4.0$

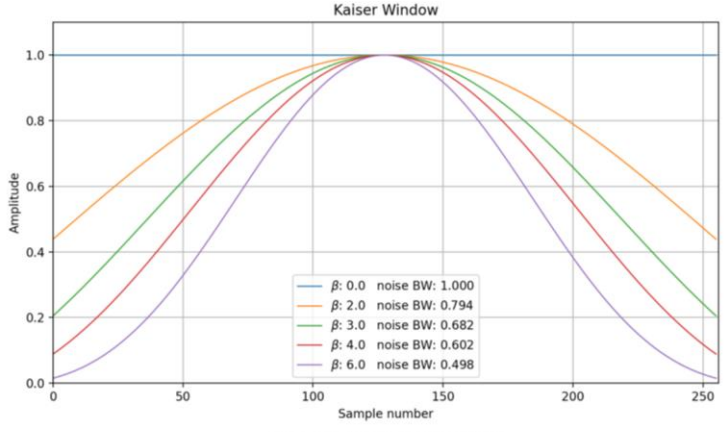

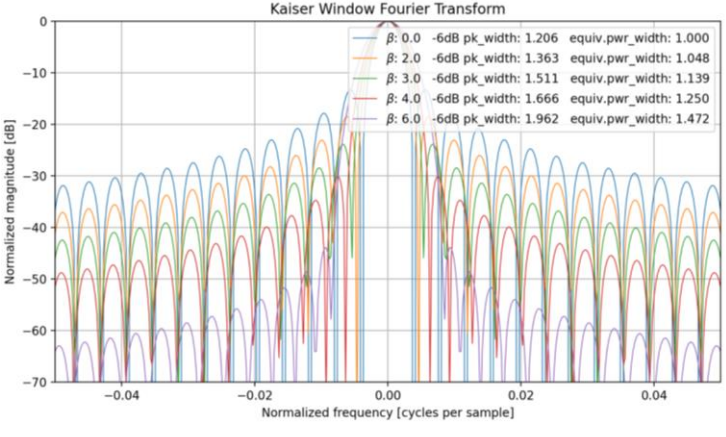

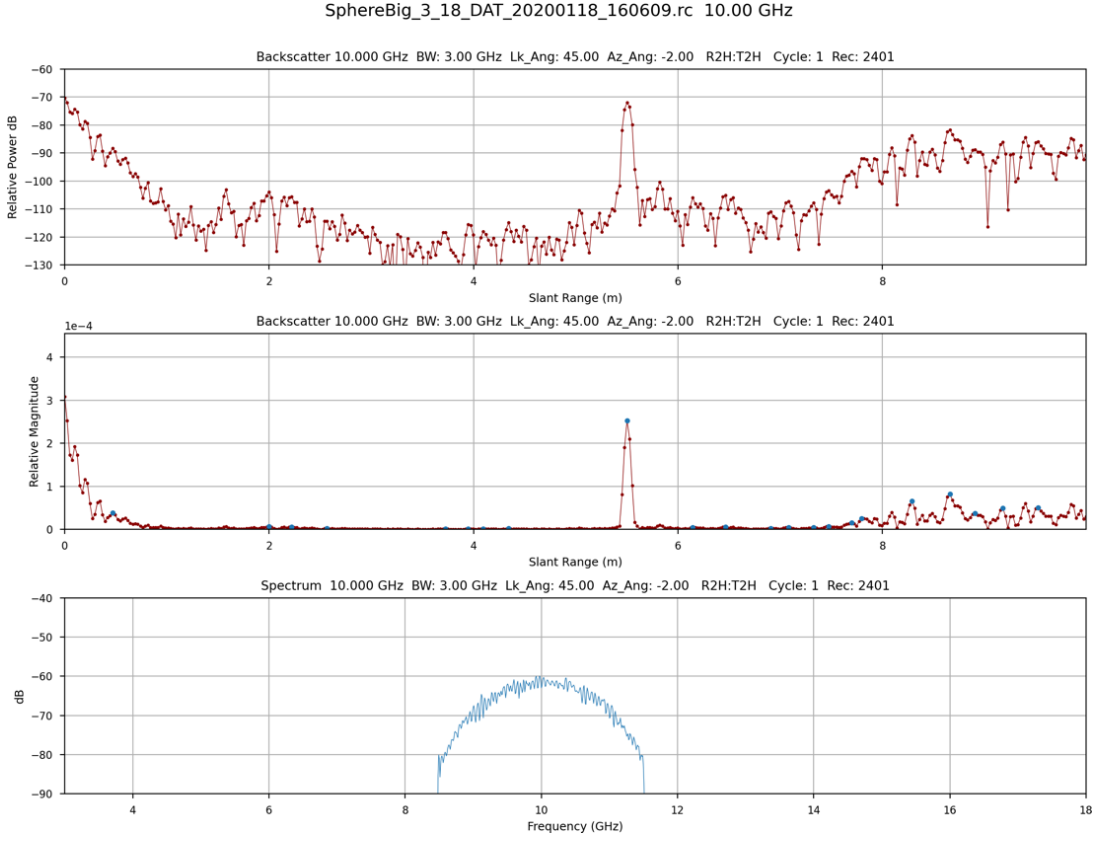

Polarimetric Calibration of WBSCAT RC Data

- Calibration algorithm derived from work or Sarabandi and Ulaby 1991
  - Assumes polarimetric isolation > 25 dB
  - Copolarized target (Sphere or Corner Reflector with known RCS)
  - Cross-pol target with high SNR (> 30 dB)
- Calibrates different gain values in the H and V channels

Figure 5-1 Stainless steel calibration sphere (47.5 cm) at Davos-Laret in 2020

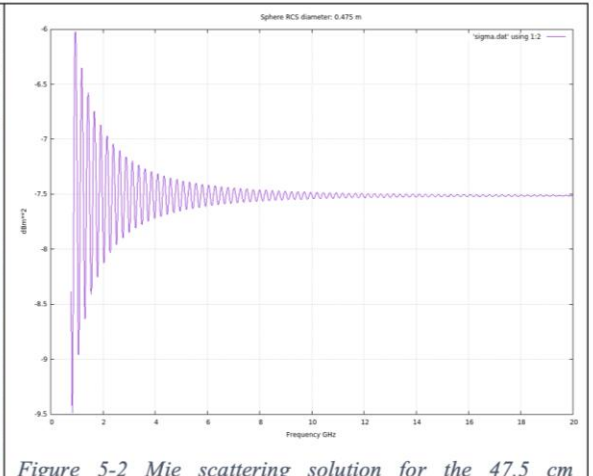

Figure 5-2 Mie scattering solution for the 47.5 cm conducting sphere

Polarimetric Calibration of Distributed Target Backscatter

- Calculating the radar backscatter coefficient σ_0 from the calibrated σ values requires determining the effective scattering surface area A_{eff}.
- The calibrated σ assumes that the scatterer is located at the center of the antenna beam, where the antenna gain is nearly constant. When there is surface scattering, the measured σ is an integral over the entire surface or volume illuminated by the antenna weighted by the 2-way relative antenna gain pattern:

$$\sigma = \frac{1}{G^2(\theta_0, \phi_0)} \int_A G^2(\theta, \phi) \sigma_0(\vec{p}) dA$$

In this integral $G(\theta, \varphi)$ is the antenna gain for each patch in the integration area, and $G(\theta_0, \varphi_0)$ is the peak gain value near the antenna boresight.

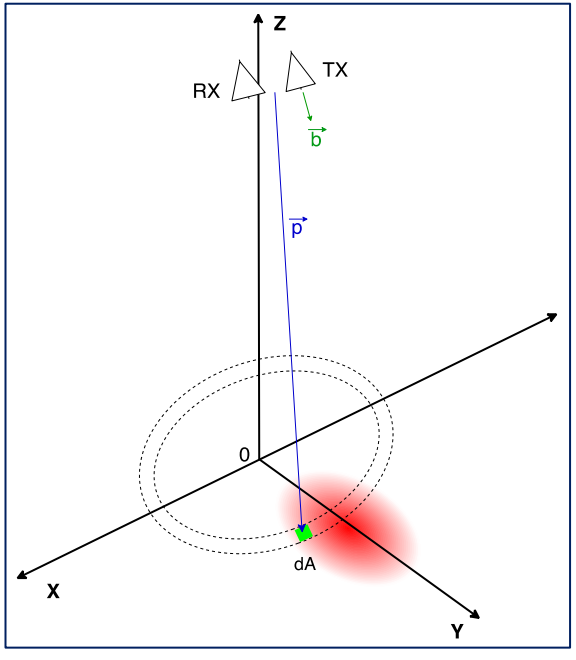

Calibration Measurements at ESTEC HERTZ Chamber

- WBSCAT at the HERTZ anechoic chamber at ESTEC, 19-26 August 2019.

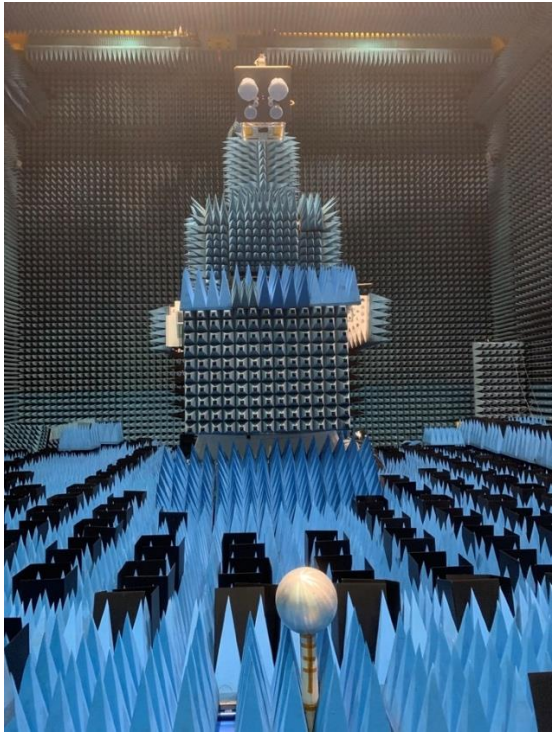

Table 1 Overview of WBSCAT measurements at the ESTEC HERTZ chamber and the scans

Target	Frequency Scans (GHz)	Scan Types
47.5 cm Sphere	1-6, 3-18, 16-40 GHz	1-D Az, El scans, 2D Big scans
40 cm Square Corner Reflector	1-6, 3-18 GHz	2D Big scans
18 cm Corner reflector	16-40 GHz	2D Big scans
25.4 cm Sphere	3-18, 16-40 GHz	2D central region small scan
40 cm Dihedral	1-6, 3-18 GHz	2D central region small scan
12 cm Polarization Grid at 45 deg. tilt	16-40 GHz	2D central small scan
20 cm Polarization Grid at 45 deg. tilt	3-18 GHz	2D central small scan
4 targets together for 3D imaging test	3-18 GHz	2D Big Scan

Calibration Sphere Measurements at ESTEC (Aug-2019)

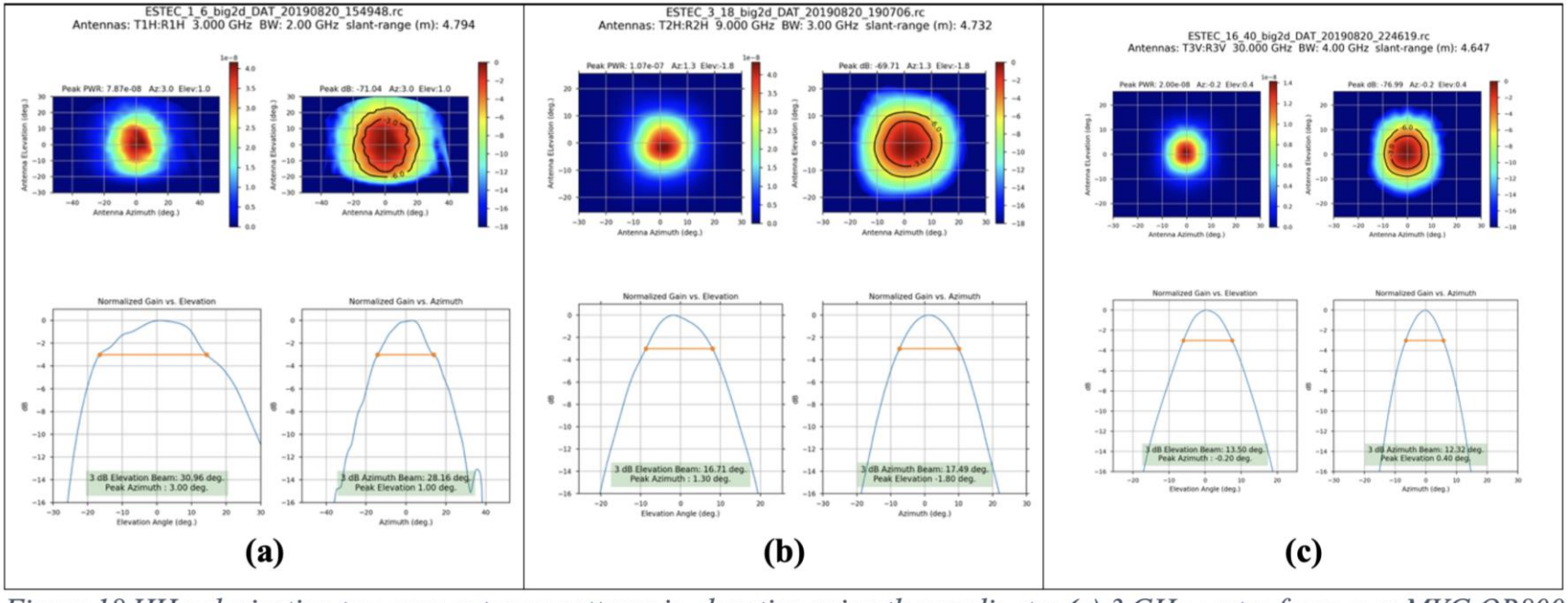

Figure 18 HH polarization two-way antenna patterns in elevation azimuth coordinates ***(a)*** *3 GHz center frequency MVG QR800 antennas* ***(b)*** *9 GHz center frequency, MVG QR2000 antennas* ***(c)****30 GHz center frequency, MVG QR18000 antennas.*

- 2D scans of the calibration targets are remapped from elevation and look angle to azimuth and elevation of the 2-way antenna pattern
- Range migration is corrected by looking for the peak of the range profile

Calibration Sphere Measurements with Phase Correction

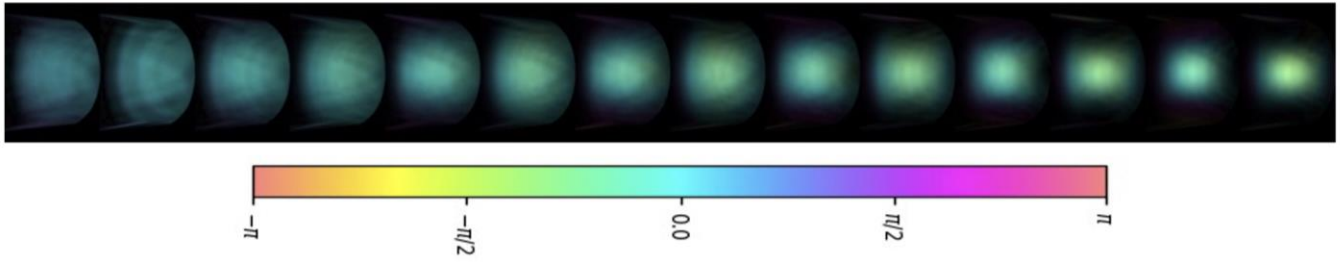

Figure 19 Calibration data from the 475 mm diameter sphere at 2,2.5,3,3.5,4,4.5,5 GHz center frequency. At each frequency the HH and the VV pattern is shown.

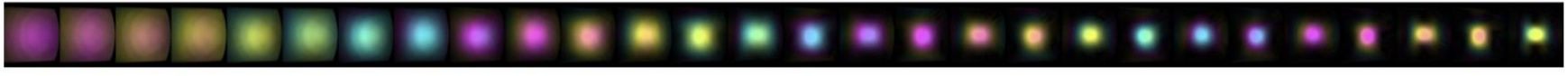

Figure 20 Calibration data from the 475 mm diameter sphere at 4.5, 5, 6, 7, 8, 9, 10, 11, 12, 13, 14, 15, 16, 16.5 GHz cente frequency. At each frequency the HH and the VV pattern is shown.

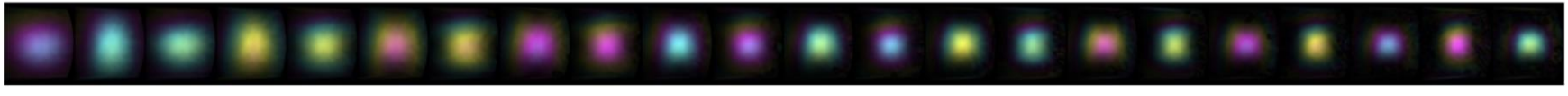

Figure 21 Calibration data from the 475 mm diameter sphere at 18, 20, 22, 24, 26, 28, 30, 32, 34, 36, 38 GHz center frequency increasing from left to right. At each frequency the HH and the VV pattern is shown

- These 2D patterns measured at ESTEC are used to calculate the effective illuminated area

Initial Campaign 2018-2020 Davos-Laret

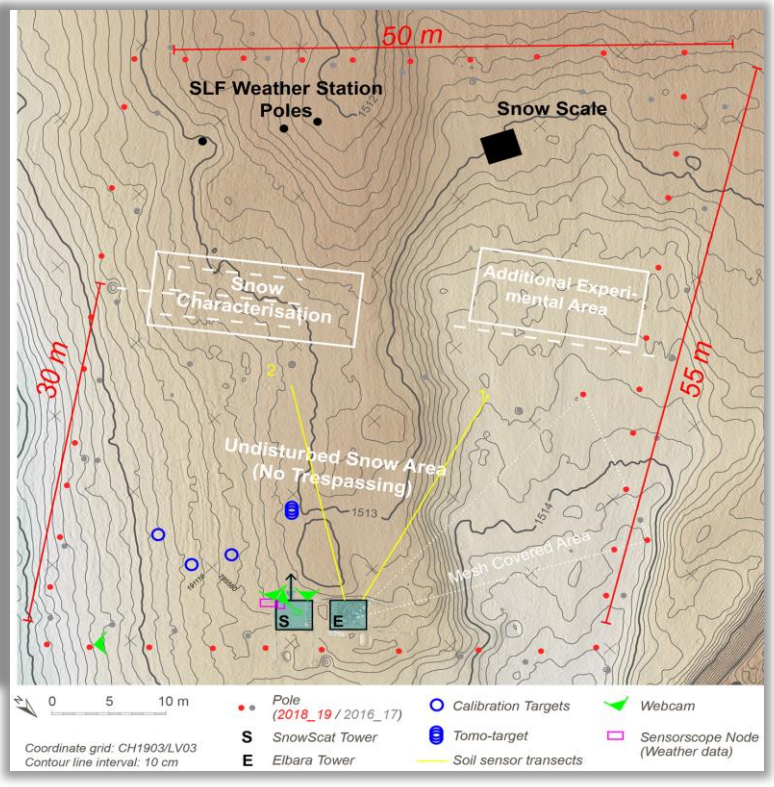

The test site for the winter 2018/2019 and 2019-2020 campaigns is located close to the village Laret on the municipal territory of Davos, in Graubunden. The elevation is 1514 meters.

Calibrated σ_0 Time-Series at Davos-Laret 2019-2020 (v3)

- Davos-Laret Time-Series at 2.5 GHz with look angles of 25, 35, and 45 degrees.

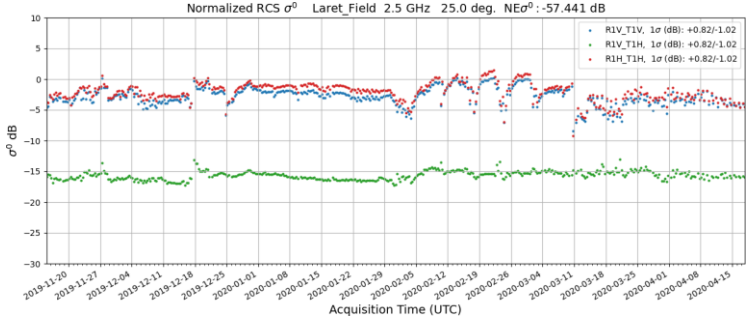

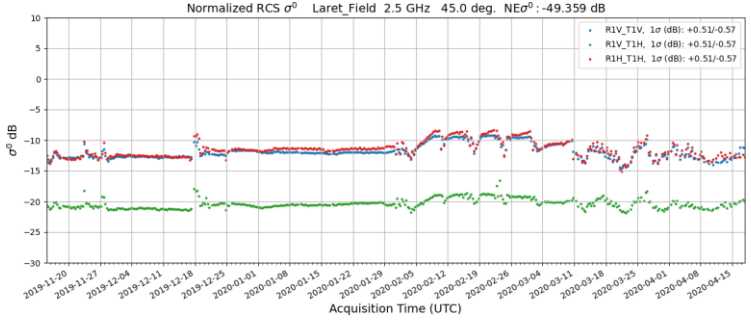

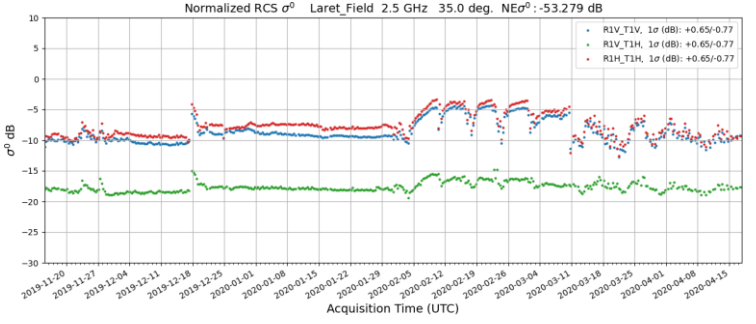

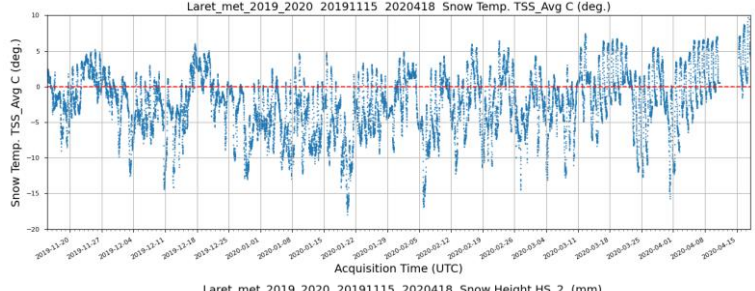

Calibrated σ_0 Time-Series at Davos-Laret 2019-2020 (v3)

- Davos-Laret Time-Series at 5.0 GHz with look angles of 25, 35, and 45 degrees

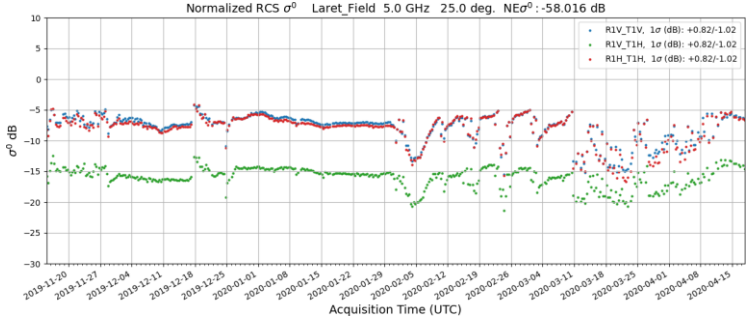

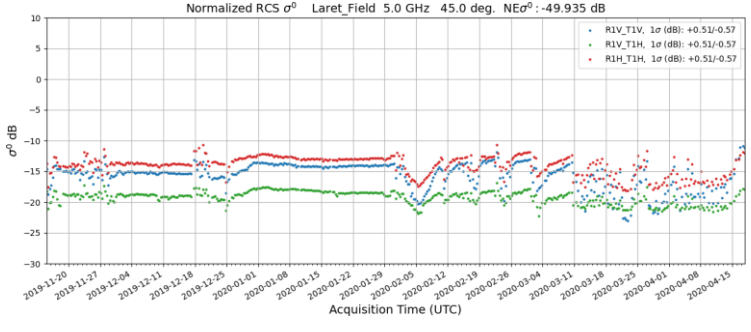

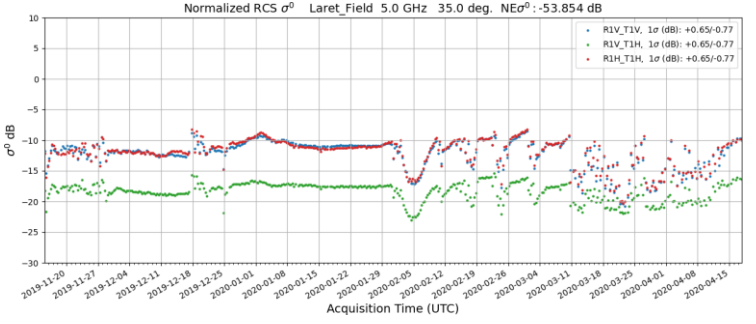

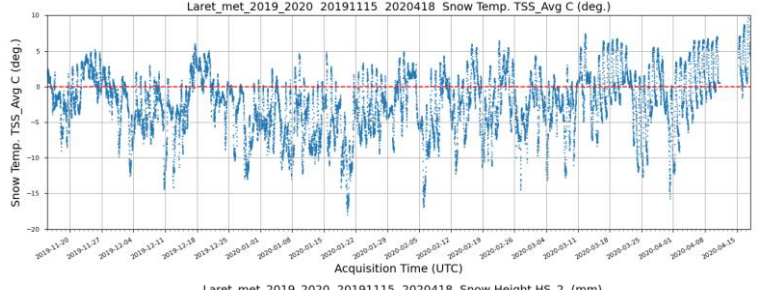

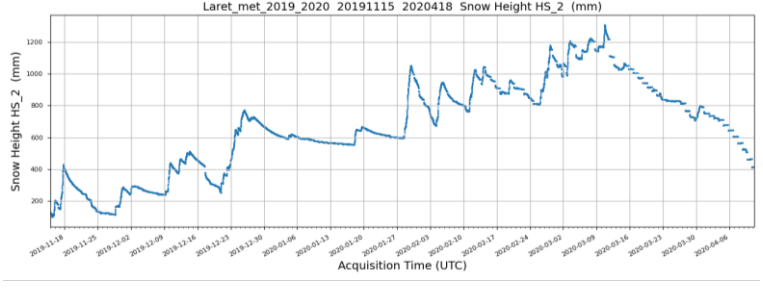

Calibrated σ_0 Time-Series at Davos-Laret 2019-2020 (v3)

- Davos-Laret Time-Series at 10 GHz with look angles of 25, 35, and 45 degrees

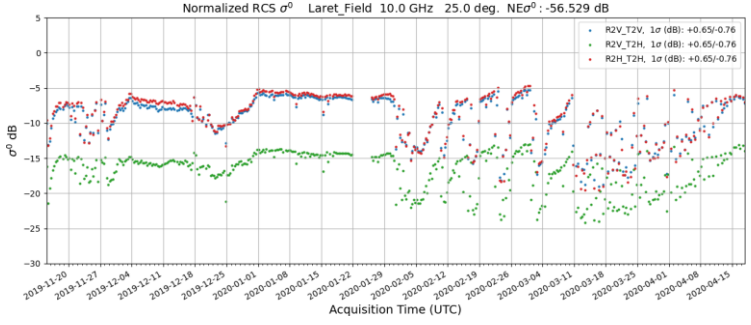

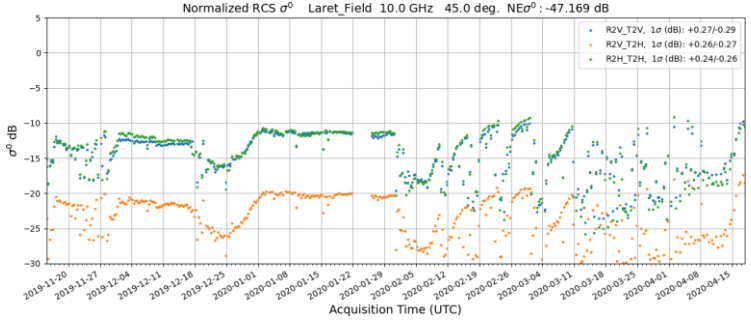

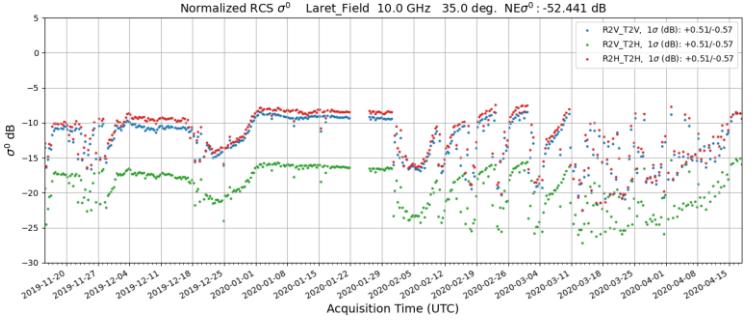

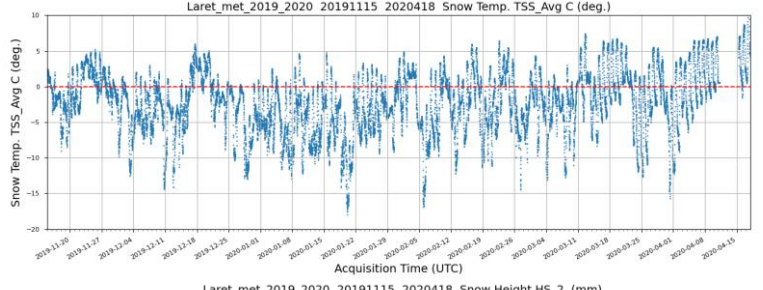

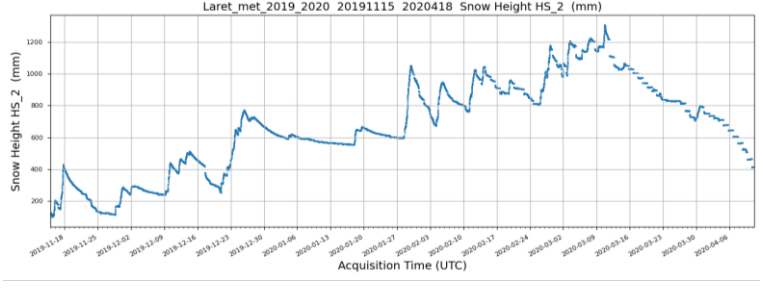

Calibrated σ_0 Time-series at Davos-Laret 2019-2020 (v3)

- Davos-Laret Time-Series at 16.5 GHz with look angles of 25, 35, and 45 degrees

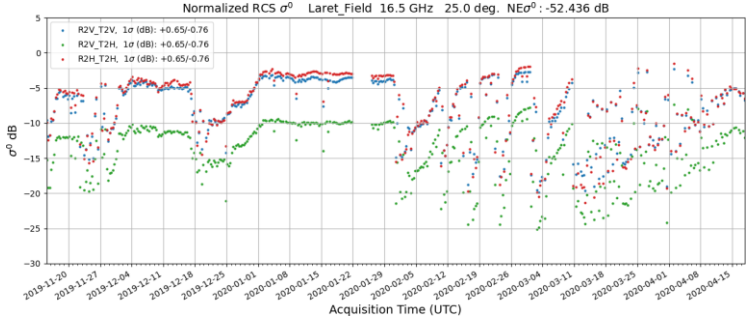

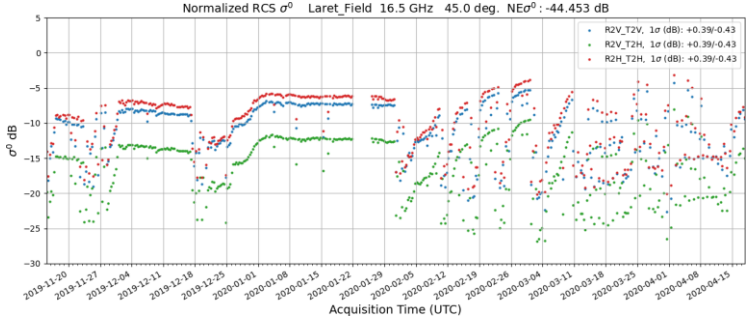

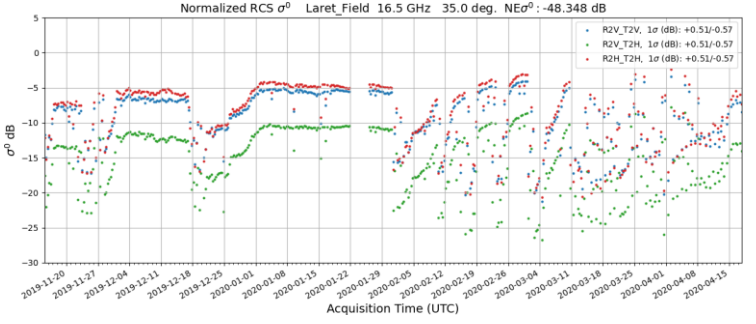

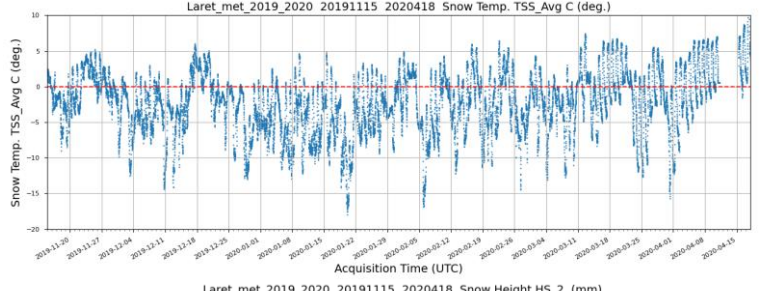

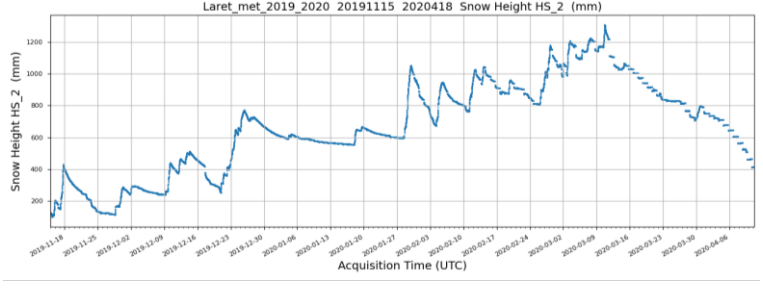

Calibrated σ_0 Time-Series at Davos-Laret 2019-2020 (v3)

- Davos-Laret Time-Series at 32 GHz with look angles of 25, 35, and 45 degrees

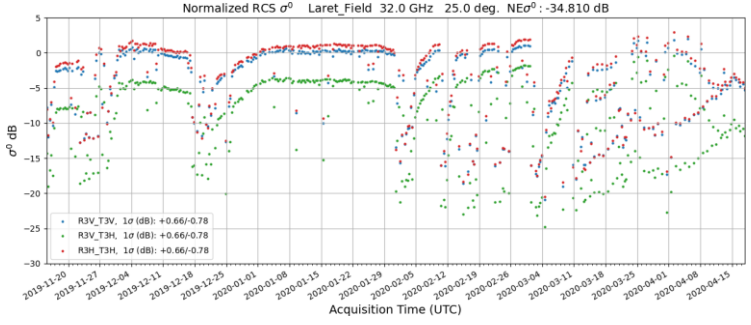

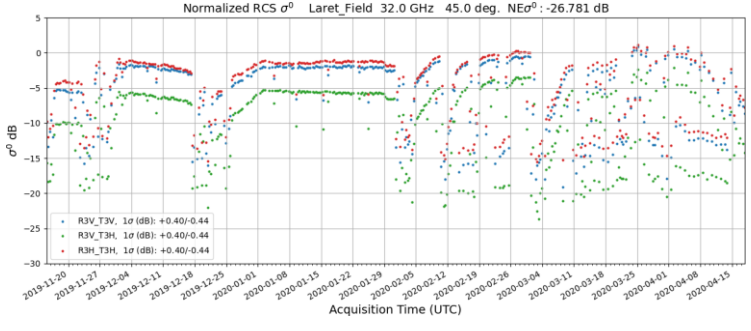

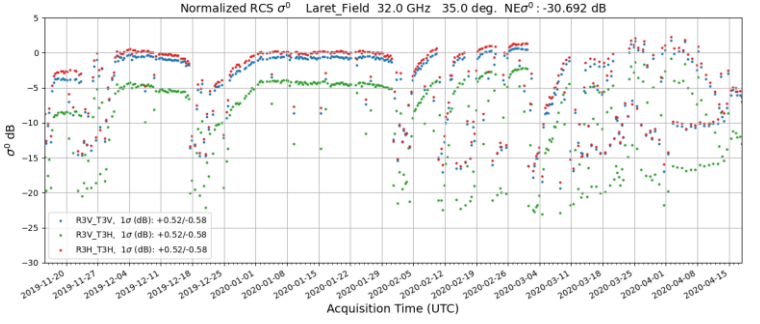

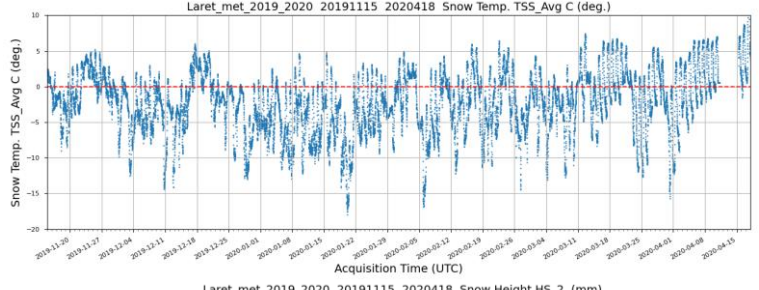

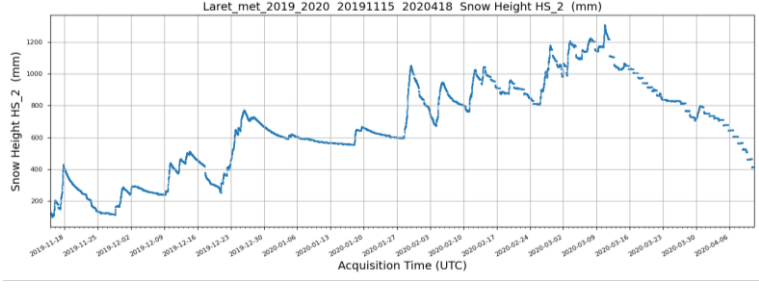

Vertical Backscatter Profiles

- Altimeter imaging geometry except close to the surface, 6-degree incidence angle

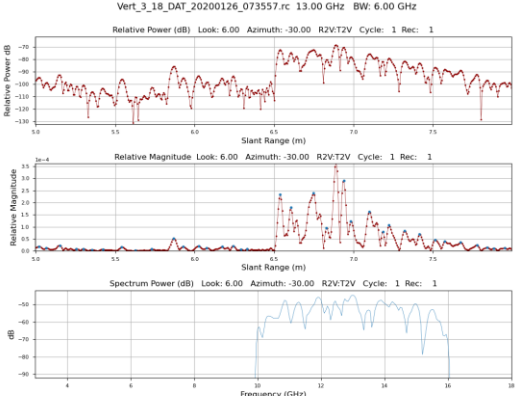

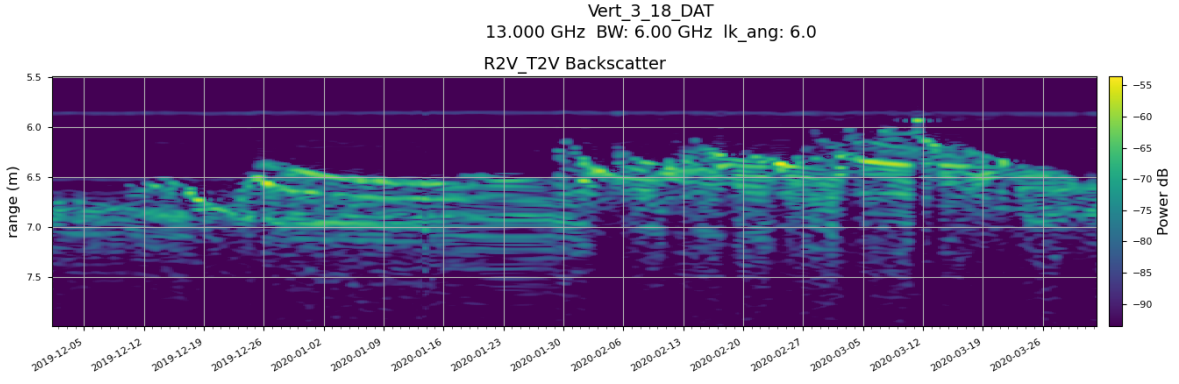

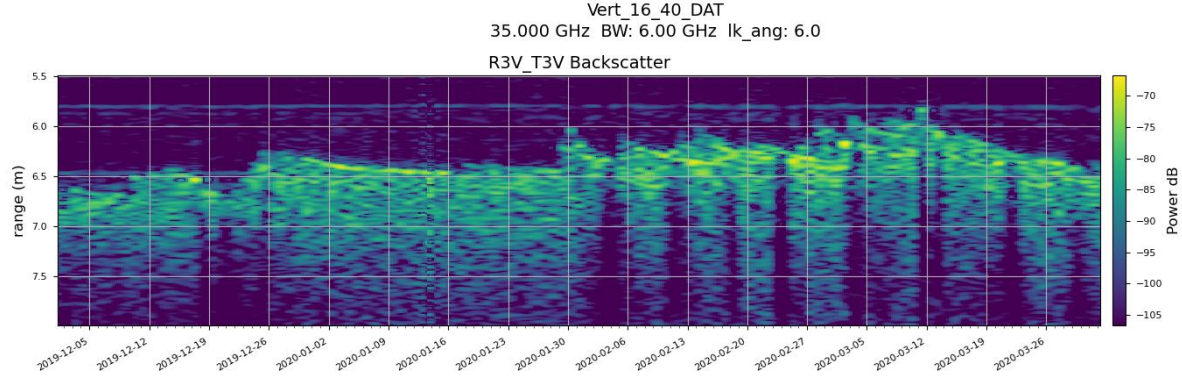

Interferometric Processing WBSCAT Data

- The SLC phase ϕ_i of a single radar scatterer is the scaled LOS distance R_i plus an offset ϕ_c that includes contributions from the radar electronics, cables, and signal processing where λ is the radar wavelength:

$$\phi_i = -\frac{4\pi R_i}{\lambda} + \phi_c \ ,$$

- Given a positive shift δ away from the radar between times t_1 and t_2, the associated differential phase change $\Delta\phi$ is defined:

$$\Delta\phi = \phi_1 - \phi_2 = \frac{4\pi\delta}{\lambda} \ .$$

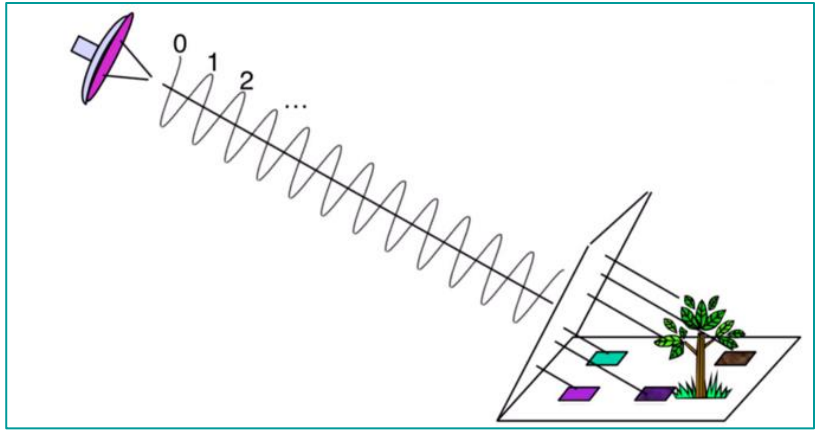

The backscatter signal contains contributions from all scatterers in the resolution element

$$z = \frac{1}{\sqrt{N}} \sum_{k=1}^{N} a_k e^{\frac{-j4\pi\rho_k}{\lambda}}$$

WBSCAT Interferogram Calculation

- Let z_1 and z_2 represent SLC values in a pair of coregistered SLC images acquired at different times t_1 and t_2. Then the normalized single-look interferogram $\gamma_{1,2}$ is defined as:

$$\gamma_{1,2} = \frac{z_1 z_2^*}{\sqrt{(z_1 z_1^*)(z_2 z_2^*)}} \; .$$

- Spatial averaging of the single-look interferogram pixels reduces phase noise due to temporal decorrelation, but also degrades the spatial resolution:

$$\bar{\gamma}_{1,2} = \frac{\overline{z_1 z_2^*}}{\sqrt{(z_1 z_1^*)(z_2 z_2^*)}} \; .$$

- The magnitude of $\bar{\gamma}_{1,2}$ is the multilook correlation coefficient and $\phi_{1,2}$ is the interferometric phase:

$$\phi_{1,2} = \arctan \frac{\Im(\bar{\gamma}_{1,2})}{\Re(\bar{\gamma}_{1,2})} \quad -\pi \leq \phi_{1,2} < \pi \; .$$

Interferometric Coherence

- The interferometric coherence $\bar{\gamma}$ is the product of the coherences from the spatial baseline γ_{sp}, thermal noise γ_n , and temporal decorrelation γ_{temp}

$$\gamma = \gamma_{sp} \times \gamma_n \times \gamma_{temp}$$

- The relationship of γ_n with respect to the SNR values of the two acquisitions in the interferogram is given by:

$$\gamma_n = \left[(1 + \frac{1}{\mathrm{SNR}_1})(1 + \frac{1}{\mathrm{SNR}_2}) \right]$$

- The Cramer-Rao bound is a good approximation for the standard deviation of the multi-look phase ϕ when the number of looks $N \geq 4$:

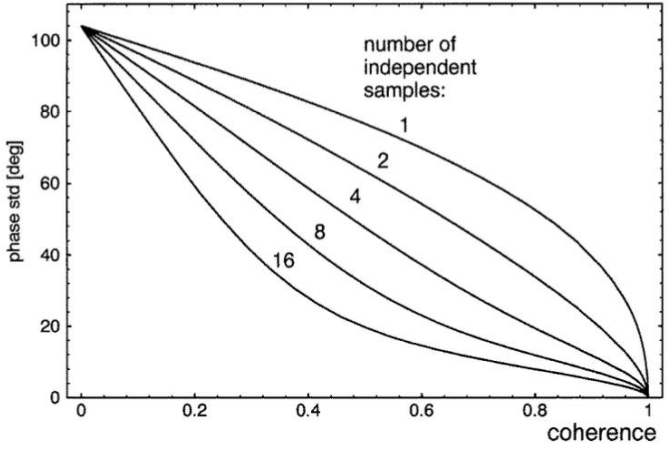

$$\sigma_\phi = \frac{1}{2N_L} \frac{1-\gamma^2}{\gamma^2}$$

WBSCAT Intensity, Interferometric Phase, and Coherence

- Intensity images and interferometric phase and coherence for 10 GHz SLC data acquired on **20200110_113559** and **2020011_1135558**
- The spatial averaging factors are by default 5 looks in range and 3 looks in azimuth

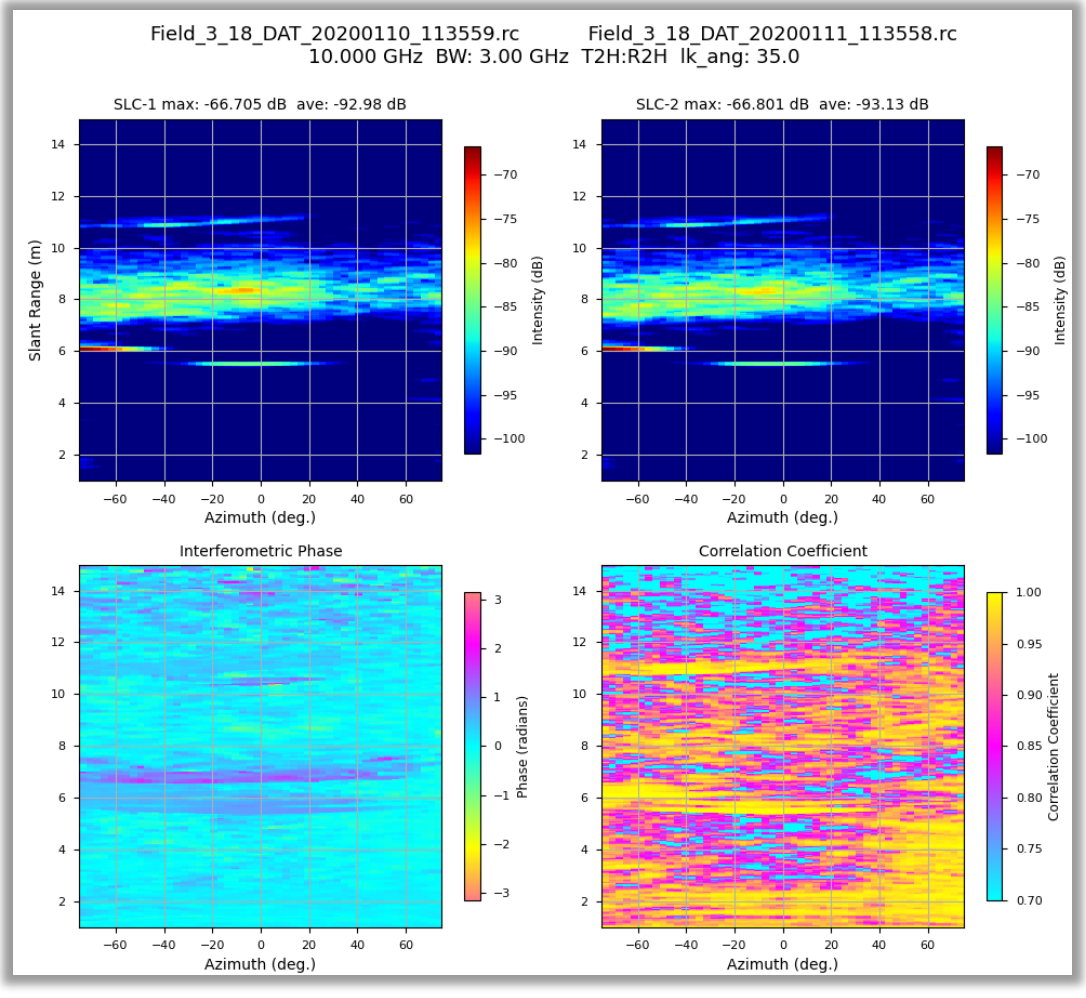

Multi-Frequency Interferometric Phase and Correlation I

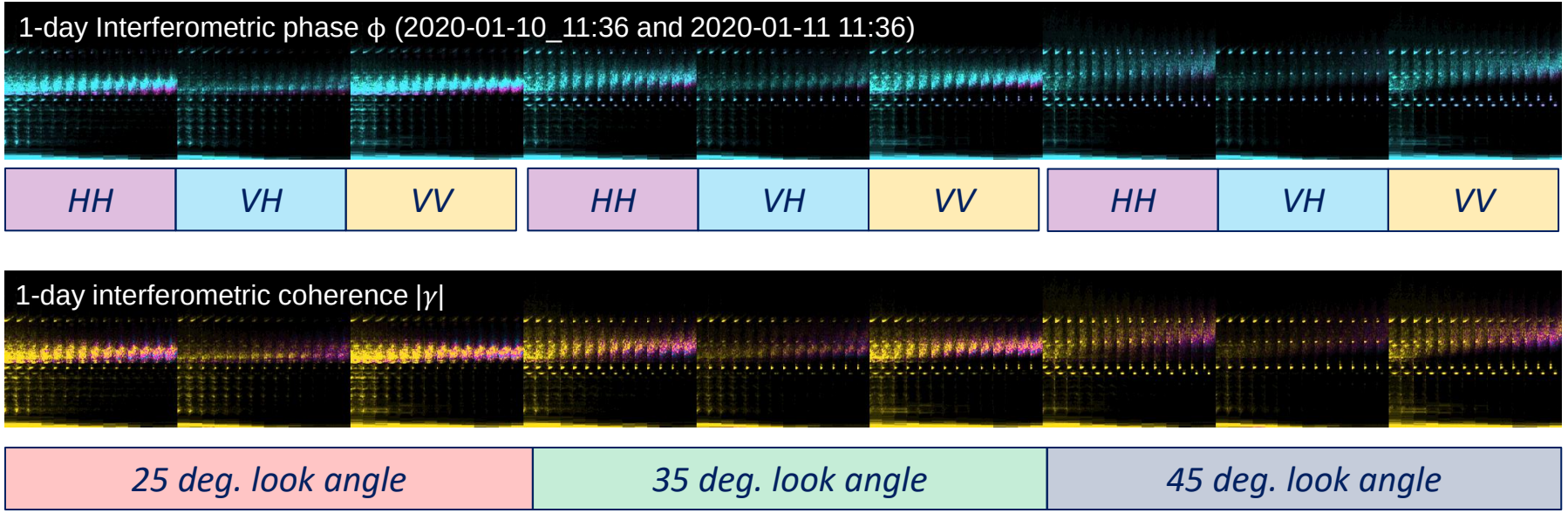

- Interferogram and correlation maps for the interferometric pair: 20200110_113559 and 20200111_113558
- There are 14 frequency sub-bands 4.5,5,6,7,8,9,10,11,12,13,14,15,16,16.5 GHz
- Each interferogram and correlation map has 51 azimuth lines, 3 degree spacing starting at -75 degrees

Multi-Frequency Interferometric Phase and Correlation II

1-day Interferogram (2020-01-10 11:36 and 2020-01-11 11:36)

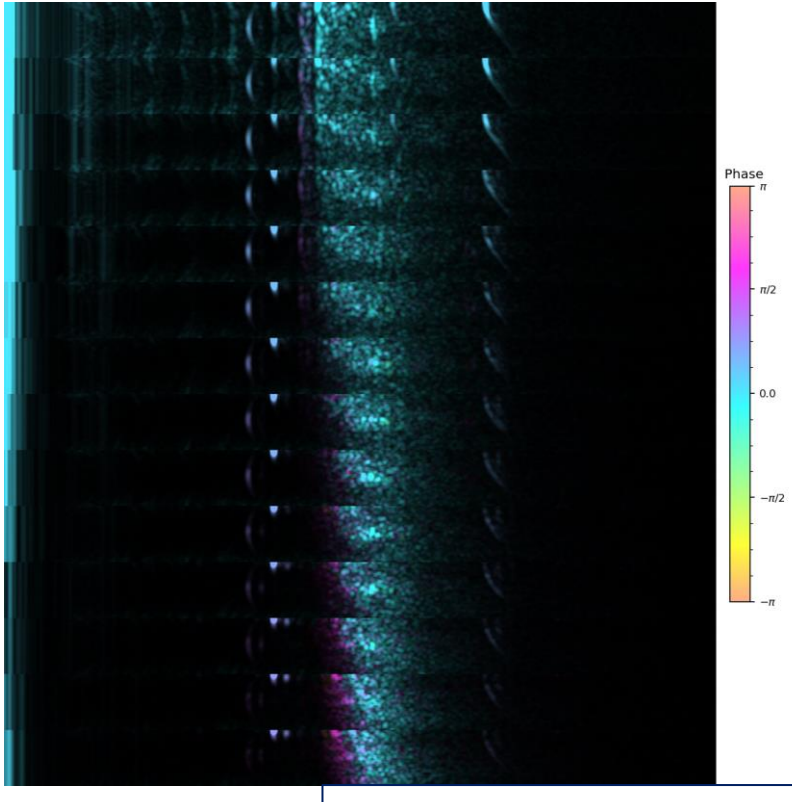

1-day interferometric correlation coefficient $|\gamma|$

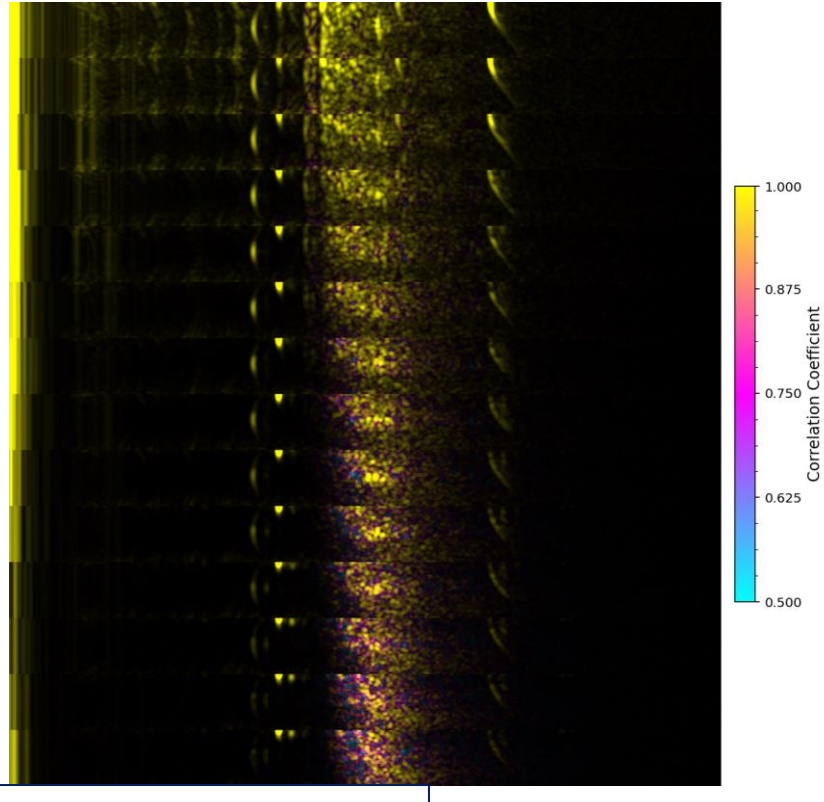

- Interferograms for HH polarization, with 35 degree look angle
- 4.5,5,6,7,8,9,10,11,12,13,14,15,16,16.5 GHz
- Interferometric pair 20200110_113559 and 20200111_113558

Coherence Time-Series: Davos Laret 2019-2020 2 GHz

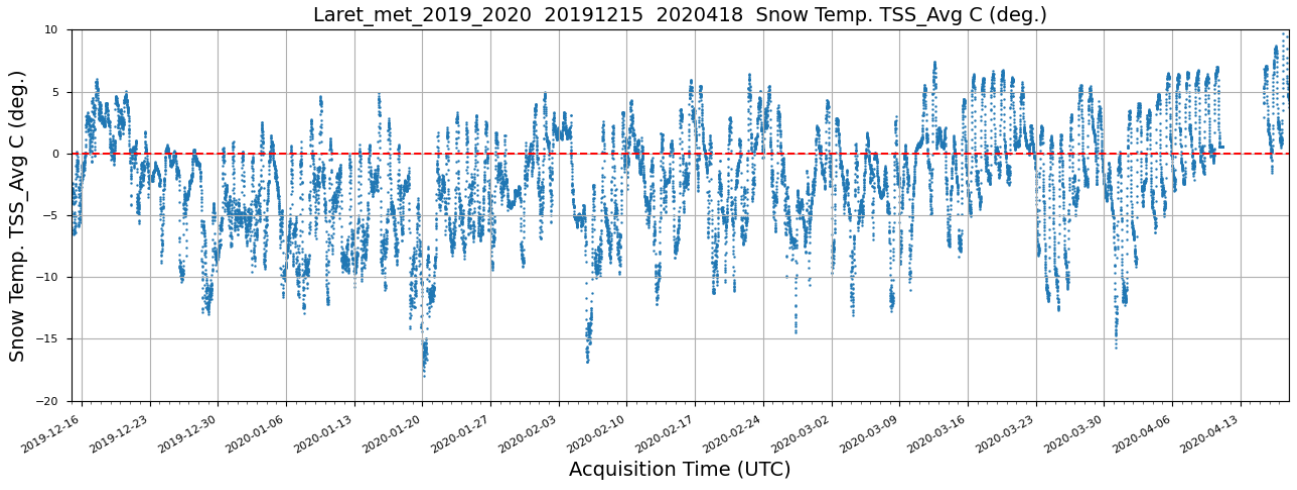

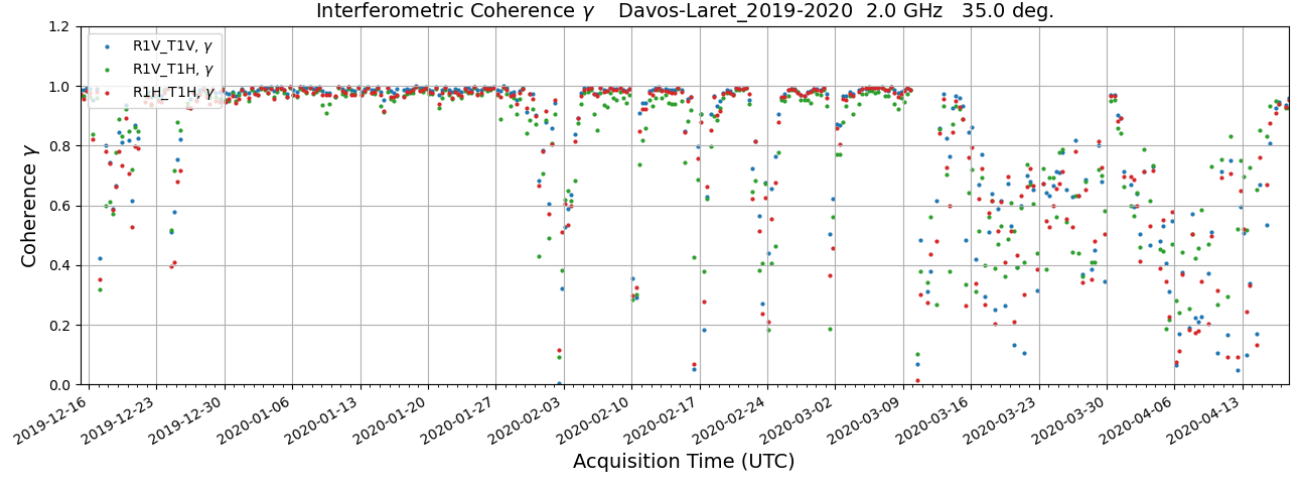

Coherence Time-Series: Davos Laret 2019-2020 5 GHz

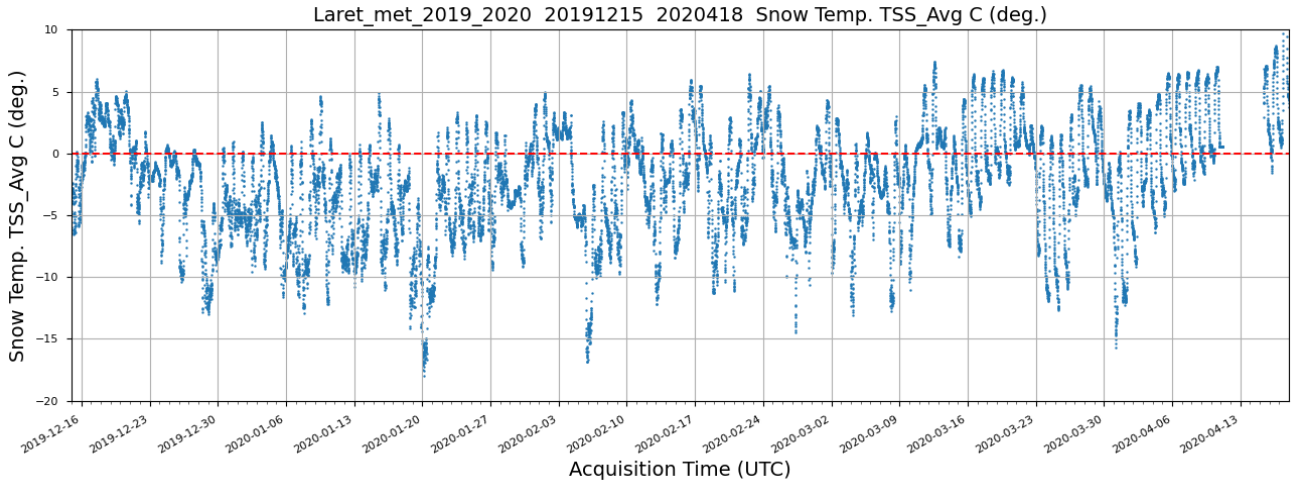

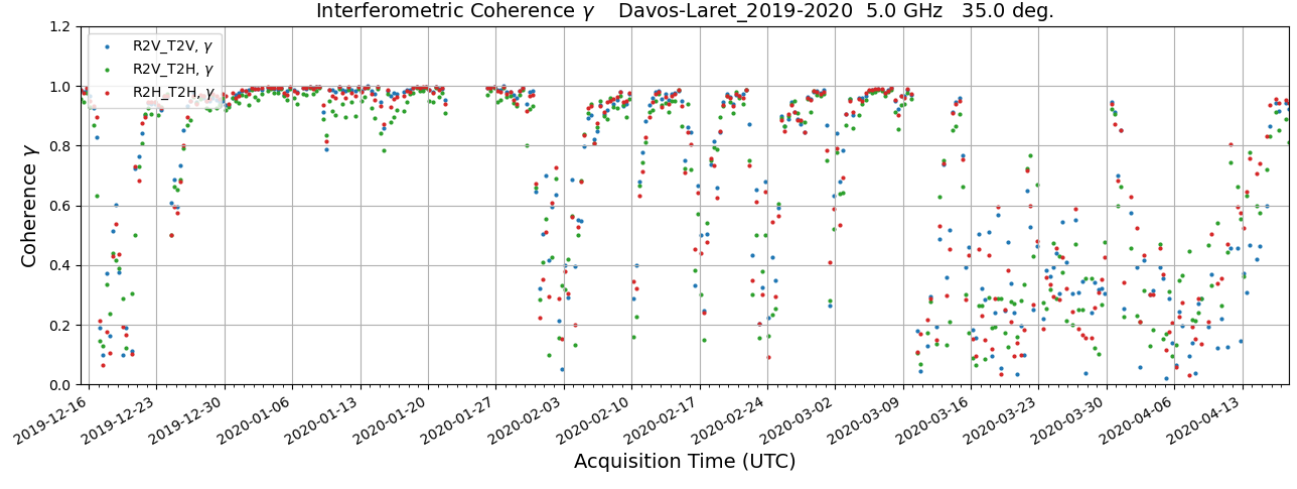

Coherence Time-Series: Davos Laret 2019-2020 10 GHz

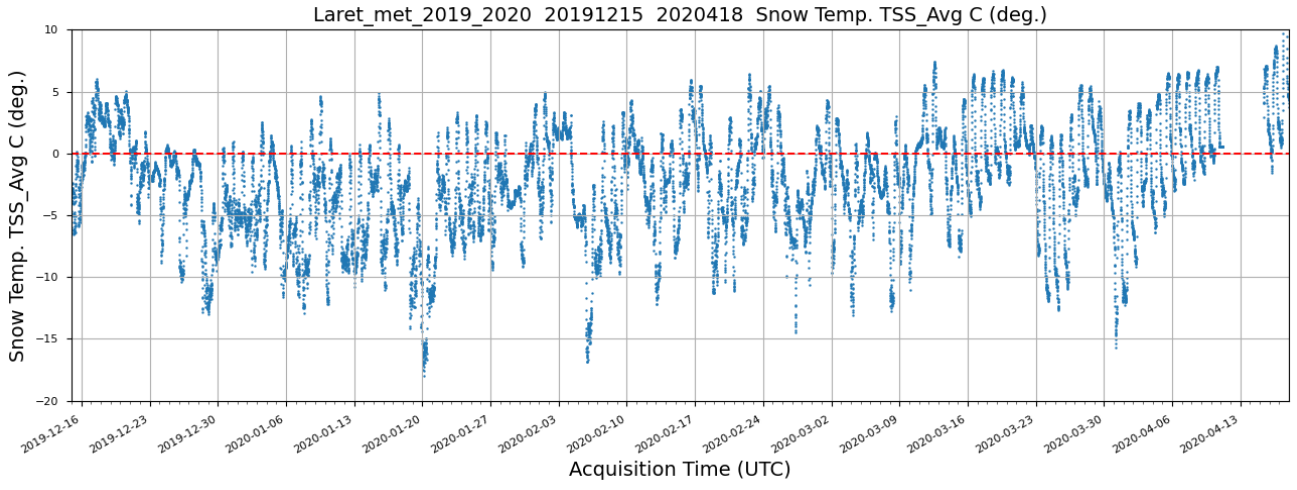

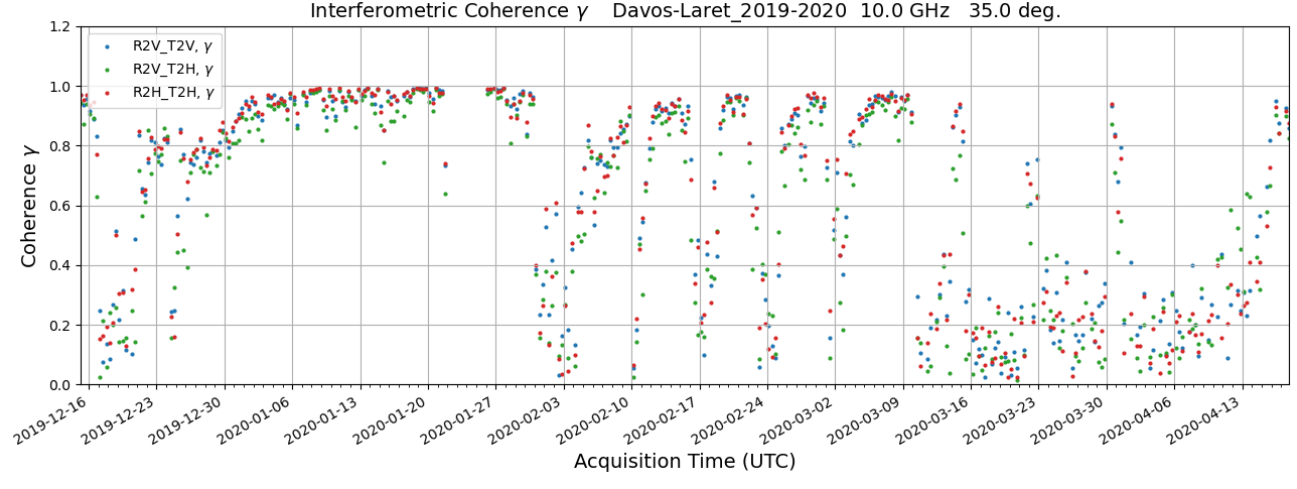

Coherence Time-Series: Davos Laret 2019-2020 13 GHz

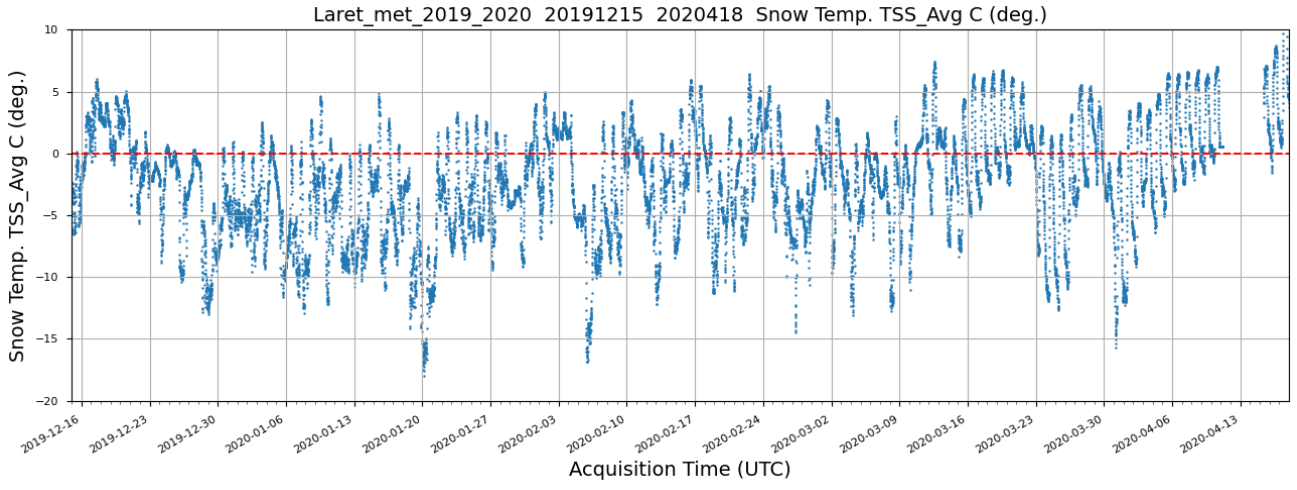

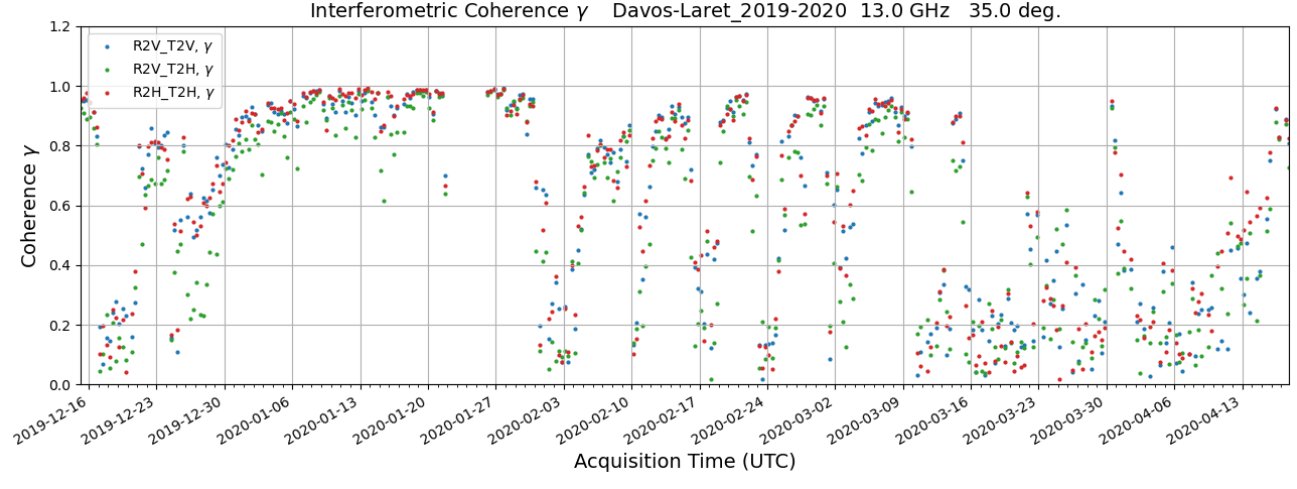

Coherence Time-Series: Davos Laret 2019-2020 32 GHz

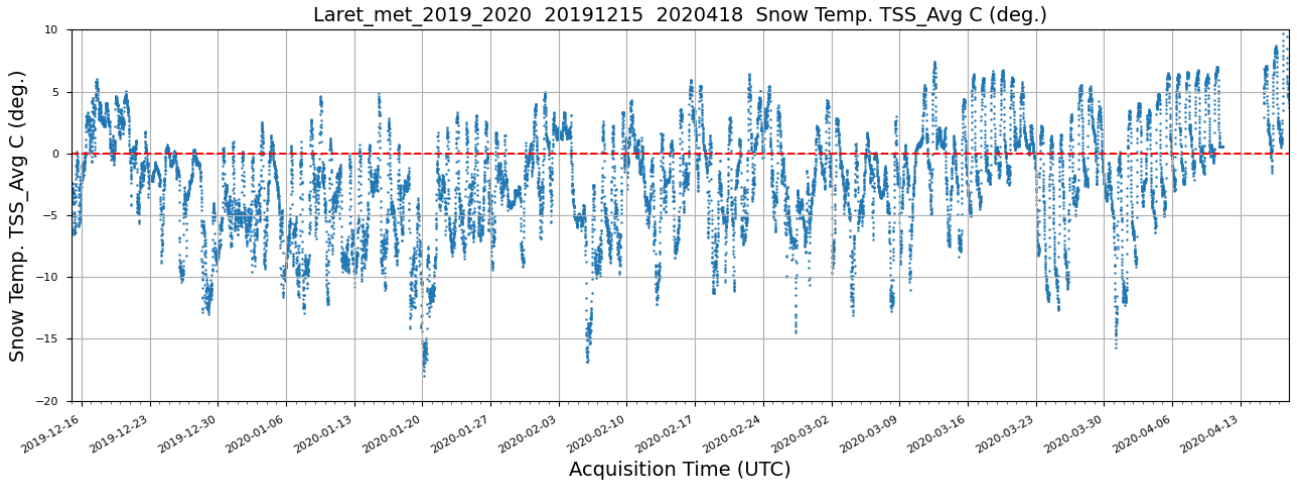

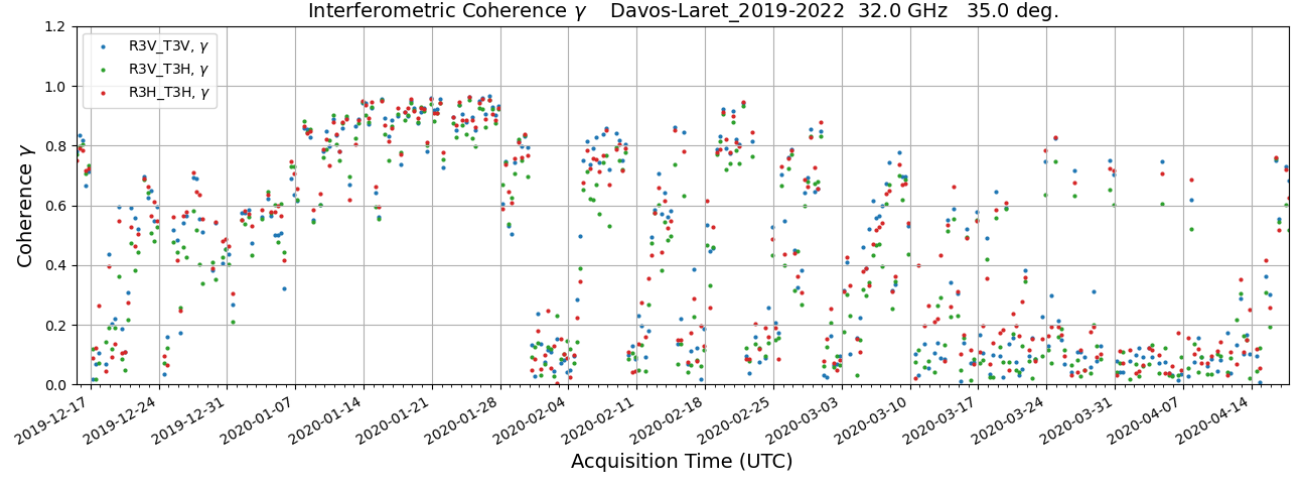

Interferometric Phase Time-Series: Davos Laret 2019-2020

Interferometric Phase Time-Series: Davos Laret 2019-2020

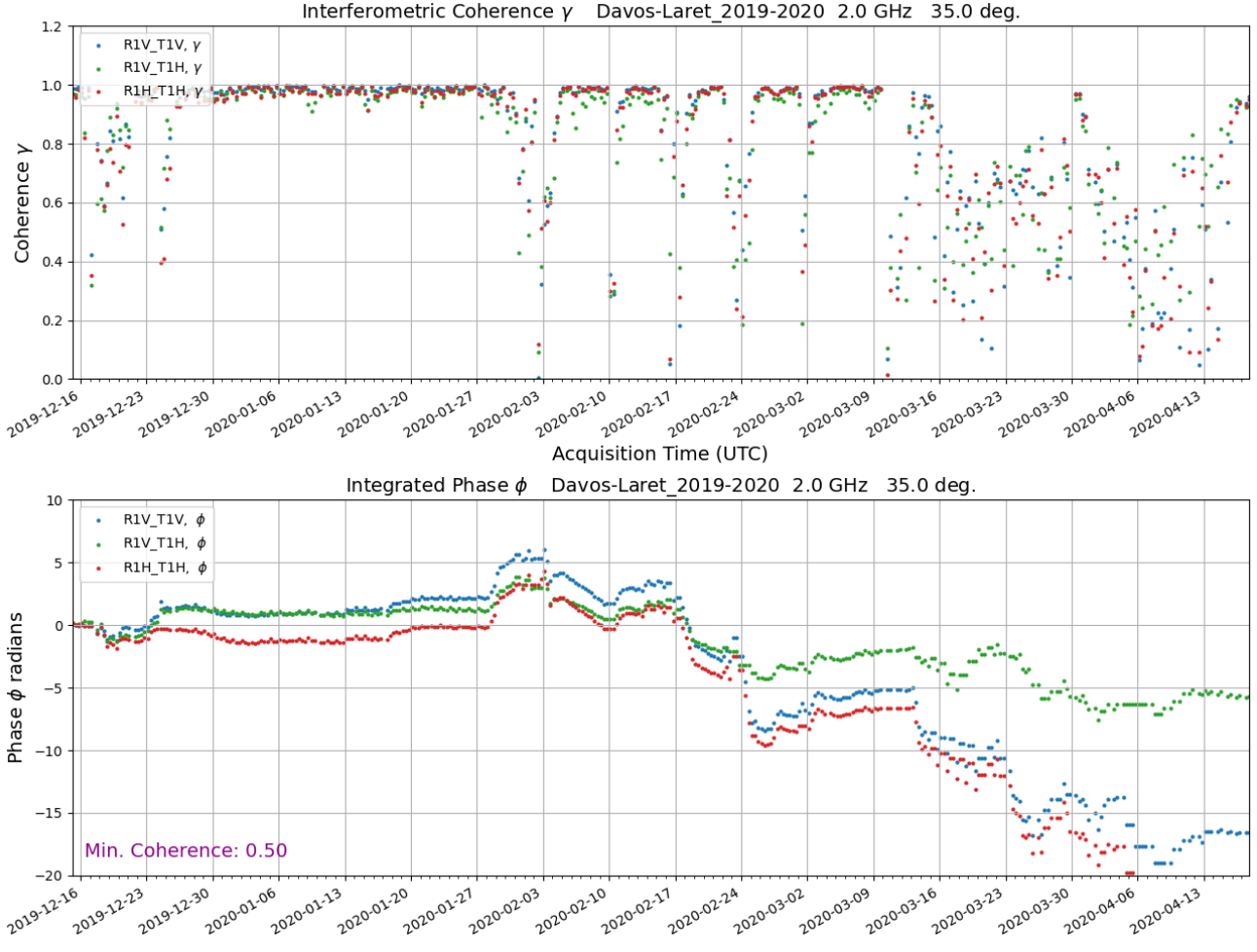

Interferometric Phase Time-Series: Davos Laret 2019-2020

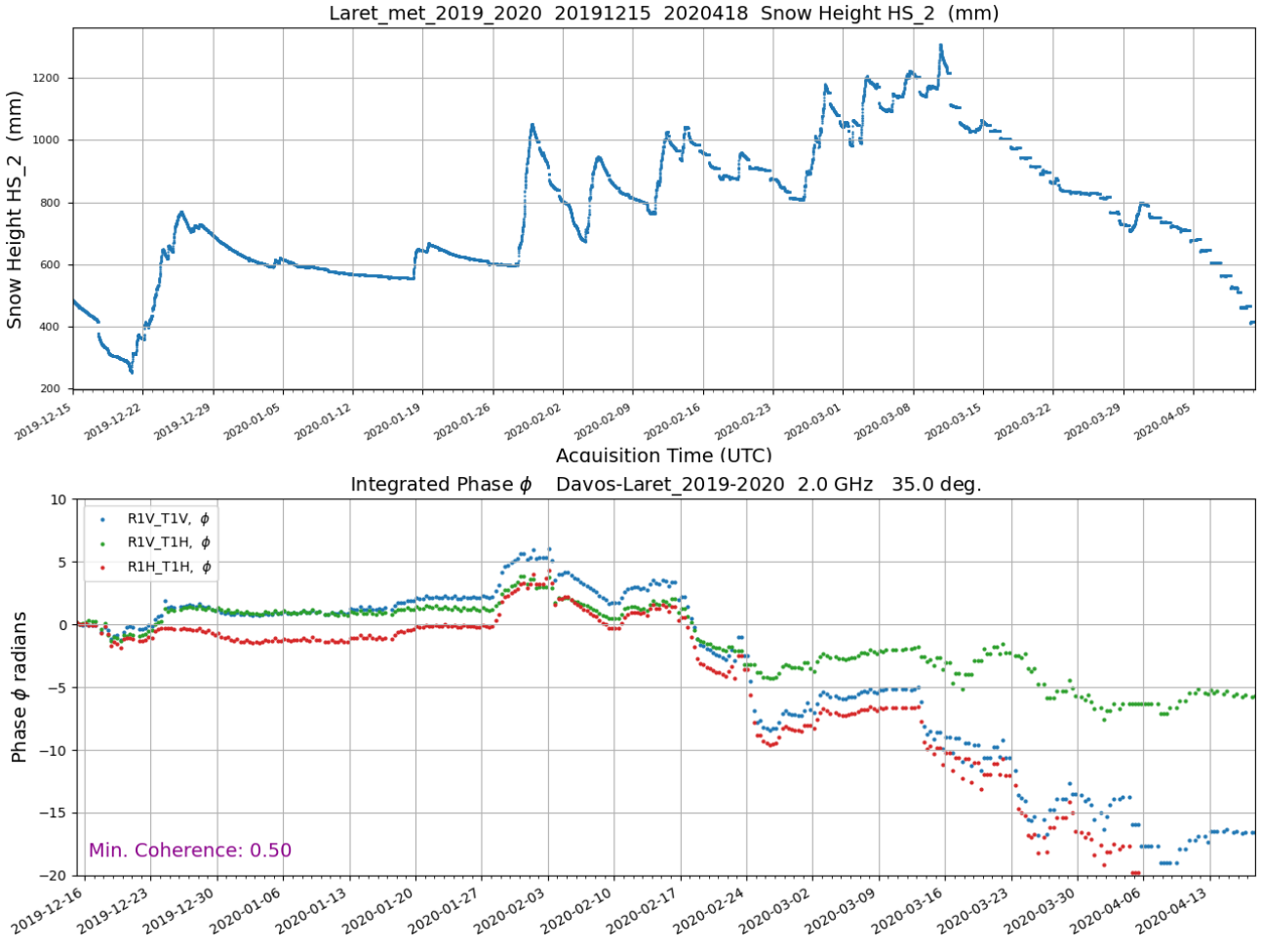

Interferometric Phase Time-Series: Davos Laret 2019-2020

Interferometric Phase Time-Series: Davos Laret 2019-2020

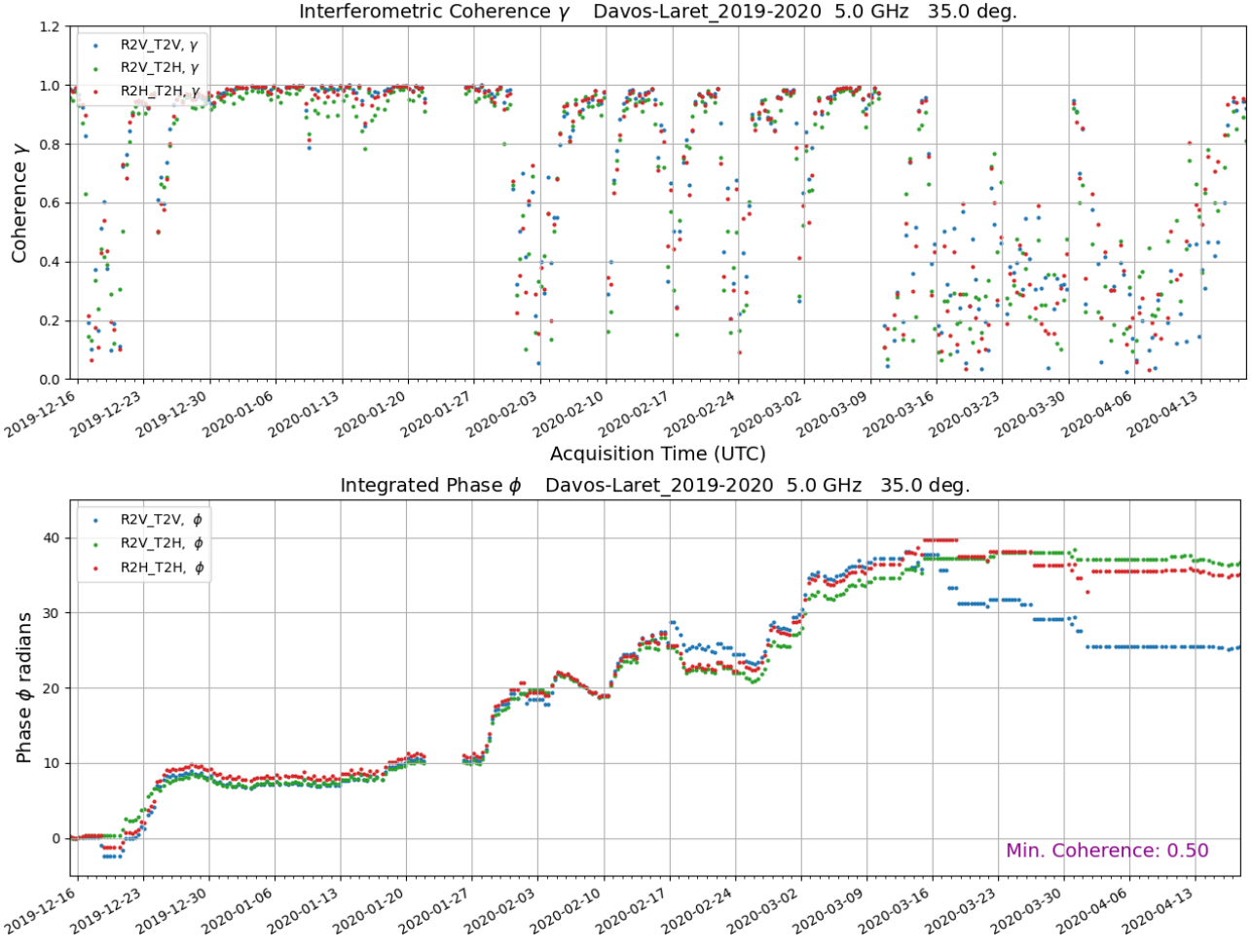

Interferometric Phase Time-Series: Davos Laret 2019-2020

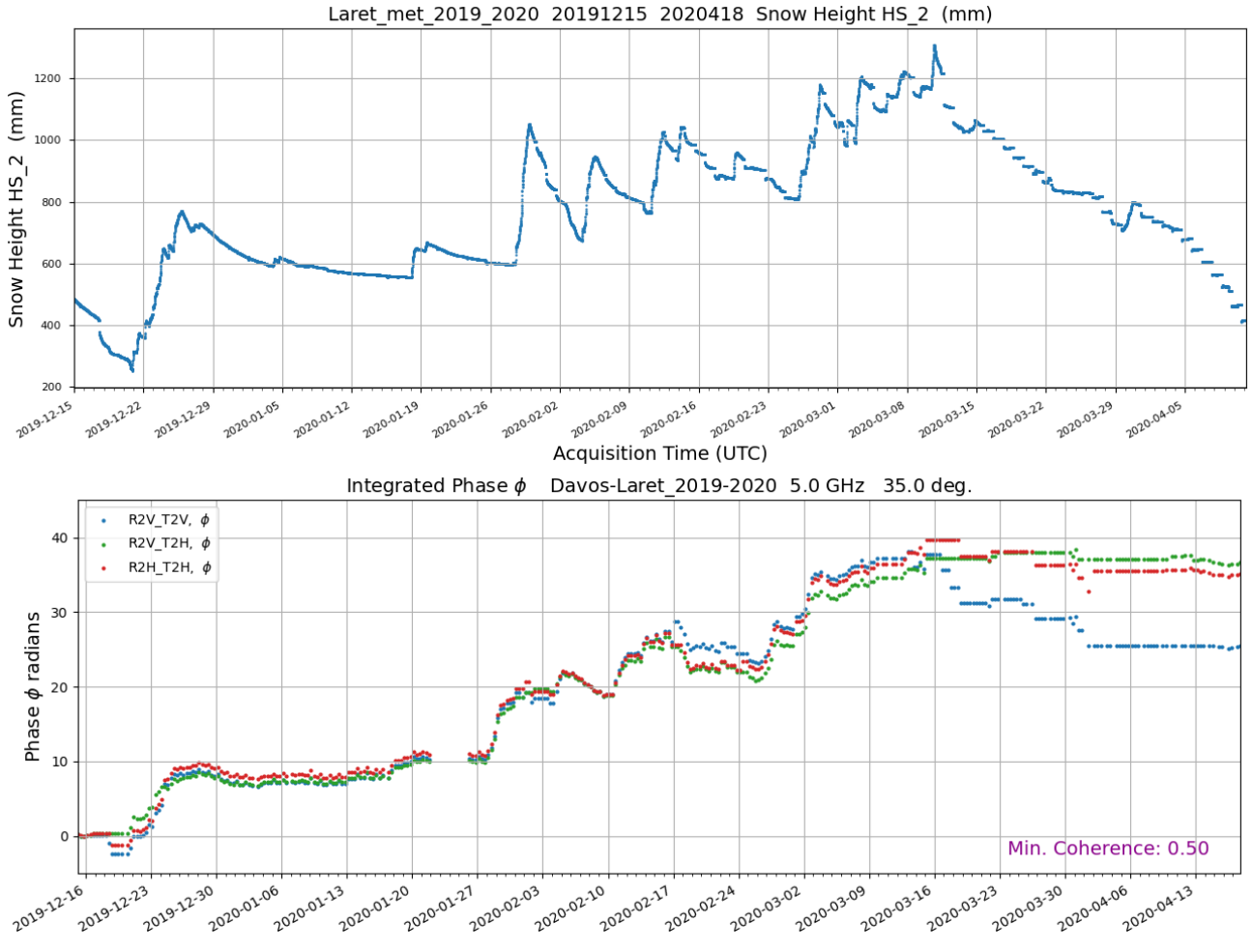

Summary

- WBSCAT acquires fully polarimetric calibrated time-series of radar-backscatter, interferometric coherence and phase in the 1-40 GHz frequency range
- Interferometric measurements of snow indicate rapid changes in the coherence and phase over 8-hour intervals during freeze/thaw periods
- Integrated interferometric phase at 2 and 5 GHz correlate with snowfall events
- Phase unwrapping errors occur during periods of low coherence and freeze/thaw
- Tomographic analysis can provide additional insight